Nuclear Instruments and Methods in Physics Research A 1072 (2025) 170148

Contents lists available at ScienceDirect

Nuclear Inst. and Methods in Physics Research, A

journal homepage: www.elsevier.com/locate/nima

Bias-induced polarization effect in $Cd_{1-x}Zn_xTe$ and $Cd_{1-y}Mn_yTe$ detectors

O. Amzallag [a,*], L. Chernyak [b], A. Ruzin [a]

[a] Faculty of Engineering, School of EE, Tel Aviv University, Tel Aviv, 69978, Israel
[b] Physics Department, University of Central Florida, Orlando, FL, 32816, USA

ABSTRACT

The study aims to compare the evolution of the electric field profiles in CdZnTe and CdMnTe detectors from the initial biasing activation until the steady state is reached (referred here as polarization effect). The crystals are grown by the same method, so the comparison emphasizes the difference between Zn- and Mn-based traps. The results demonstrate that the settling times in the CdZnTe and CdMnTe devices differ, but both are on the scale of hours. The effect of these, rather moderate variations on the charge collection efficiency for gamma photons should be limited. In addition, based on experimental results and TCAD calculations, it can be conjectured that a much stronger change in the electric field is induced by the bias polarization process in the front interface layer, which affects the charge collection only when carrier-generation occurring in and around the interface.

The alloys of II-VI groups' materials have been extensively studied for gamma detector applications, such as medical imaging, security imaging, etc. [1–4]. While the published studies on CdTe based detectors include results on polarization phenomena, the latter was mostly studied by virtue of irradiation, and not due to biasing [5]. This study compares the bias-induced polarization effects in CdZnTe (CZT) and CdMnTe (CMT) detectors grown by the same method [2,6]. Both compounds owe the high resistivity to deep-level compensation processes (Fermi-level "pinning") [7], and therefore, they contain high densities of deep traps. Changes in the occupancy of such traps affect the electric field distribution and it may also affect the carriers' lifetimes.

Both $Cd_{0.85}Zn_{0.15}Te$ and $Cd_{0.93}Mn_{0.07}Te$ crystals $(20 \times 20 \times 5\ mm^3)$ used in this study, were grown by a modified horizontal Bridgman method [2,8] and were supplied by GE Healthcare [9]. Planar M-S-M devices were obtained by thermal evaporation of indium contacts on both sides of each crystal. For resistivity measurements 0.25 cm^2 area contacts with guard rings were used to avoid the impact of the surface leakage, while for TCT measurements ~0.7 cm^2 area contacts were used (for more uniform electric field). Low bias current-voltage characterization of the $Cd_{0.85}Zn_{0.15}Te$ and $Cd_{0.93}Mn_{0.07}Te$ "guarded" devices (namely, contacts with biased guard-rings) reveal practically linear curves as presented in Fig. 1.

Resistivities of the materials can be estimated from low-bias slopes of the I–V curves, and geometry. The resistivity of $Cd_{0.85}Zn_{0.15}Te$ is estimated to be $2 \bullet 10^{10}$ Ωcm, and that of $Cd_{0.93}Mn_{0.07}Te$ $1 \bullet 10^{10}$ Ωcm. For electric-field calculations, TCT (transient current technique) was utilized. It should be noted that the contacts used for TCT had higher currents due to larger area and lack of biased guard-rings, but the SNR was sufficient. Laser pulses (λ = 640 nm, duration ~ 25 ns) were used to generate the transient current pulses. The current pulses measured in the external circuit by the TCT system were dominated by the displacement currents caused by the excess electrons (positive potential was applied to the back electrode). Fig. 2 exhibits TCAD simulation results for a TCT characterization of a 1 mm thick $Cd_{0.85}Zn_{0.15}Te$ M-S-M device. The electron-hole (*e-h*) pairs are generated mainly within a couple of μm from the front contact (FC), as shown by the simulation in Fig. 2(a). An ideal ohmic contact maintains thermodynamic equilibrium (TDE) densities at the interface, thus it recombines all the excess carriers, whereas an ohmic contact with finite recombination velocity (v_R) only partially recombines the excess carriers at the interface. This is indicated on the excess-electron density snapshots at various times after the laser pulse, by different gradients of electron-densities near FC for $v_R \rightarrow \infty$ and $v_R = 10^5$ cm/s, in Fig. 2(a). Thus, a substantial fraction of the laser-generated electrons recombines on the front contact during and following the laser pulse due to diffusion. In fact, analyzing the various current components at the FC for 1000 V/cm field, we find that *most* of the laser-generated electrons recombine on the FC, and only a small fraction (denoted $N_e(0)$) participate in the current signal, as shown in Fig. 2(b). This fraction increases with increasing external electric field intensity, and it decreases with laser power (plasma effect).

The electric field was reconstructed from the measured current pulses [10]. The measured pulses were deconvoluted from the systems' transfer function, and the calculation process on the resulting current signals was modified to account not only for the trapping effect, but also for finite laser pulse duration, and partly to account for electron

* Corresponding author.
E-mail addresses: odelyaa@mail.tau.ac.il, odlyamza@gmail.com (O. Amzallag).

https://doi.org/10.1016/j.nima.2024.170148
Received 3 July 2024; Received in revised form 13 November 2024; Accepted 3 December 2024
Available online 4 December 2024
0168-9002/© 2024 Elsevier B.V. All rights reserved, including those for text and data mining, AI training, and similar technologies.

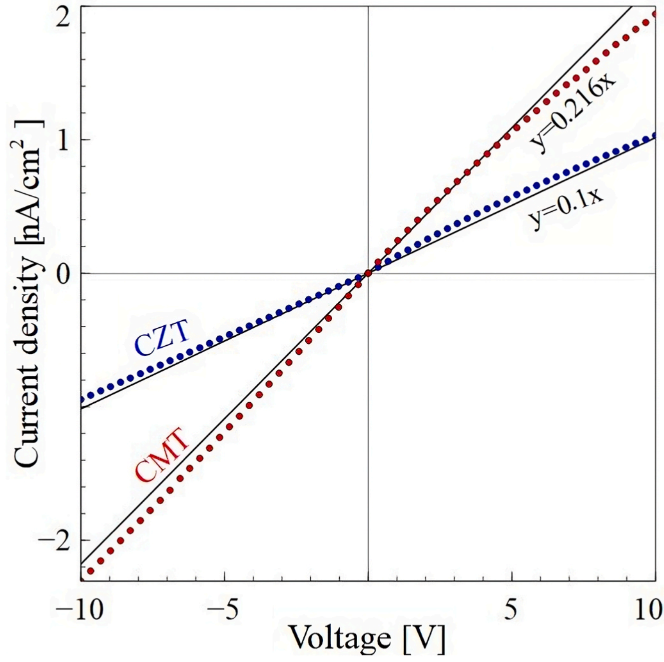

Fig. 1. Low voltage I–V curves of the $Cd_{0.85}Zn_{0.15}Te$ and $Cd_{0.93}Mn_{0.07}Te$ devices with biased guard-rings. Experimental results are marked by dots, and near-zero linear fits are marked by solid lines.

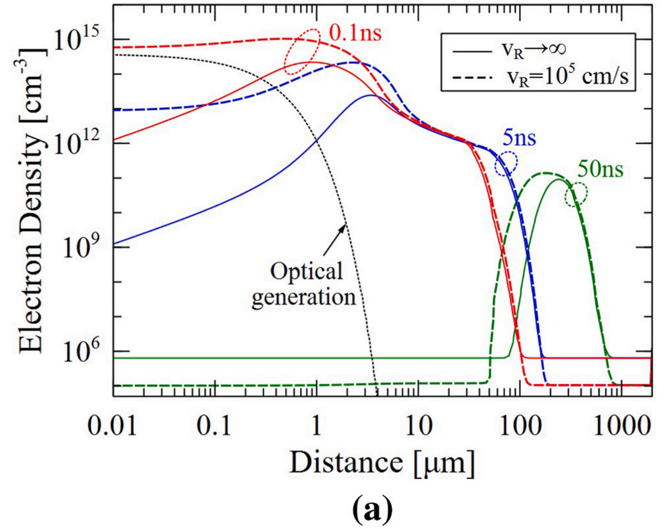

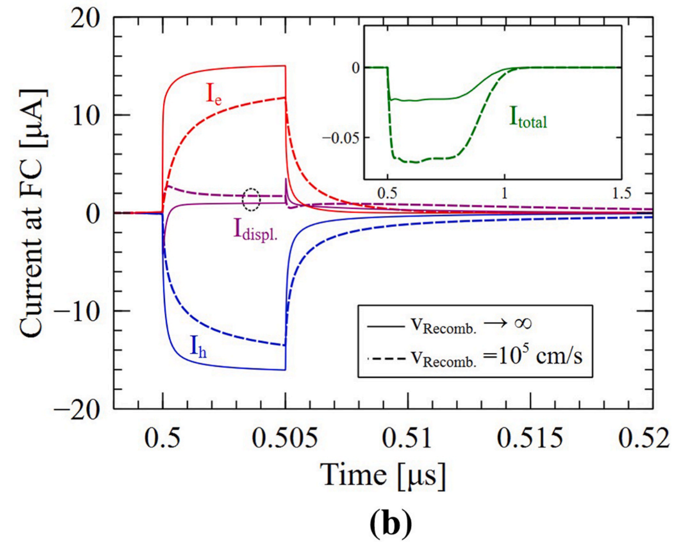

Fig. 2. TCAD simulation results for a 1 mm thick $Cd_{0.85}Zn_{0.15}Te$ device with ohmic contacts biased at $V_{FC} = -100$ V, and laser illuminated for 5 ns with $\lambda =$ 640 nm photons. Calculations for a front contact with infinite recombination velocity ($v_R \to \infty$ [cm/s]) and for $v_R = 10^5$ [cm/s] are represented by solid and dashed curves, respectively. (a) excess electron distribution at various times *after* the laser pulse ends; (b) current components on the front (negatively biased) electrode (FC).

diffusion during the drift. The electron lifetimes, τ_e, were evaluated from the current pulses obtained for *low bias voltages* $(|V|\langle 500V <)$. At such conditions the current pulse width is independent of the bias voltage, indicating that the current ends due to charge trapping and recombination, rather than due to the recombination of the excess electrons on the back contact. This is illustrated in Fig. 3, by current pulse integration (collected charge) as a function of time. For bias voltages below ~600 V the amplitude of the charge signal increases, but the time of drifting remains (marked by circles in the inset of Fig. 3). It is noteworthy that under such conditions there is a substantial element of ambipolar transport (namely, the excess electrons and holes are not fully separated by the external field). Therefore, in addition to trapping by deep-level the excess carriers are subject to recombination. The resulting "combined" lifetime may be substantially lower than the commonly used one (which is the trapping lifetime).

The lifetimes of the electrons in $Cd_{0.85}Zn_{0.15}Te$ and $Cd_{0.93}Mn_{0.07}Te$ were estimated at approximately 245 ns, and 135 ns, respectively, and they do not change notably after polarization. Due to the above-mentioned partial electron recombination on the front contact, the "initial" number of the excess electrons contributing to the current, $N_e(0)$, is unknown. The calculation of the electric field can be performed without knowing $N_e(0)$ or electron mobility, by normalizing the integral of the electric field to the applied voltage, and the thickness of the active region to the physical device thickness (assuming the electric field at high bias voltage extends throughout the bulk).

The current pulses in the CZT and CMT detectors were measured periodically starting 10 s after the initial bias activation (−600 V or −700 V on FC) until they reached a steady state. The total light budget of the TCT measurements was minimized by optimizing the laser pulse power and duration versus the required number of averages, to avoid light-induced polarization. The electric field profiles obtained for −600 V and −700 V bias voltages until stabilization are shown in Fig. 4. For convenience, different Y-axes are drawn for −600 V and −700 V bias voltages.

In the results shown in Fig. 4 the stabilization time for $Cd_{0.93}Mn_{0.07}Te$ devices was reached after 20 h, whereas for

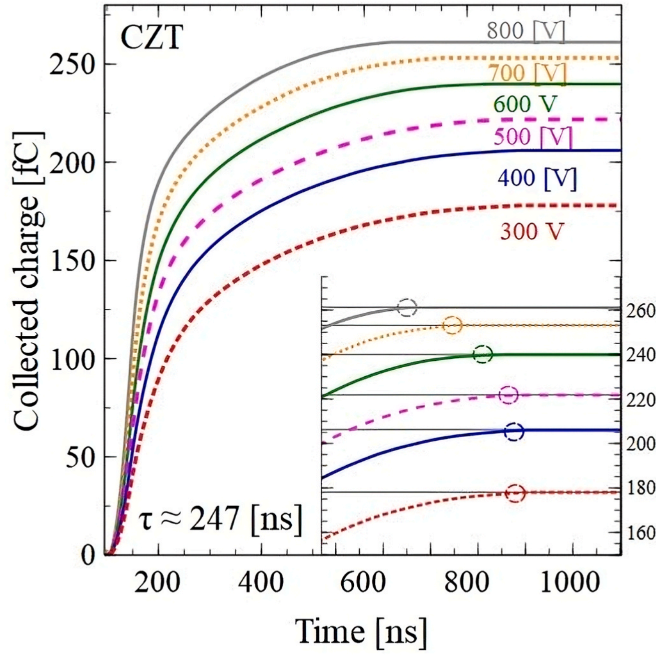

Fig. 3. Integrals of deconvoluted TCT current pulses, representing the total collected charge as a function of time. It this example the results were obtained for $Cd_{0.85}Zn_{0.15}Te$ devices. The inset zooms on the saturating curves' parts.

$Cd_{0.85}Zn_{0.15}Te$ devices it was reached after 6 h. Both $Cd_{0.85}Zn_{0.15}Te$ and $Cd_{0.93}Mn_{0.07}Te$ devices recovered from the final (steady) state to the initial state after ∼16 h at zero bias. While for electric field calculations, we use normalized current pulses (only the shape matters), it is interesting to note that the amplitude of the deconvoluted current pulses increased significantly with polarization. For convenience this is demonstrated by the collected charge (integrated current pulses) before and after reaching the steady state, in Fig. 5. The inset shows a corresponding example of current pulses for CZT devices. Due to differences in contact thickness and reflection in CZT and CMT devices, quantitative comparison of the collected charge between the devices is impossible, however the comparison before and after polarization in each device is meaningful.

There are two possible reasons for the charge increase after polarization: CCE has improved significantly or $N_e(0)$ has increased. The electric field distribution in most of the bulk did not change dramatically, and the lifetime did not change notably. Thus, it can be concluded that most probably $N_e(0)$ has increased. As mentioned above, simulations indicate that less excess electrons recombine on the front contact for higher electric fields (stronger drift surpasses diffusion in the interface layer). Thus, higher $N_e(0)$ at steady state is likely to indicate a stronger electric field in the generation area. It is important to stress that while we calculate the E-field in most of the bulk volume from the TCT pulses, the electric field in the frontmost region cannot be extracted in our setup (due to laser pulse duration and plasma effect). Thus, the most probable (indirect) explanation for the increase of the current pulses after bias-induced polarization is that the polarization forms a narrow region ($\sim \mu m$) of a strong electric field under the front electrode, which leads to the reduction of electron recombination on the front contact. This is totally feasible, since this region features by far the highest densities of both excess electrons and holes. In addition, such a μm layer of high electric field would not affect notably the potential distribution in the rest of the 5 mm thick bulk.

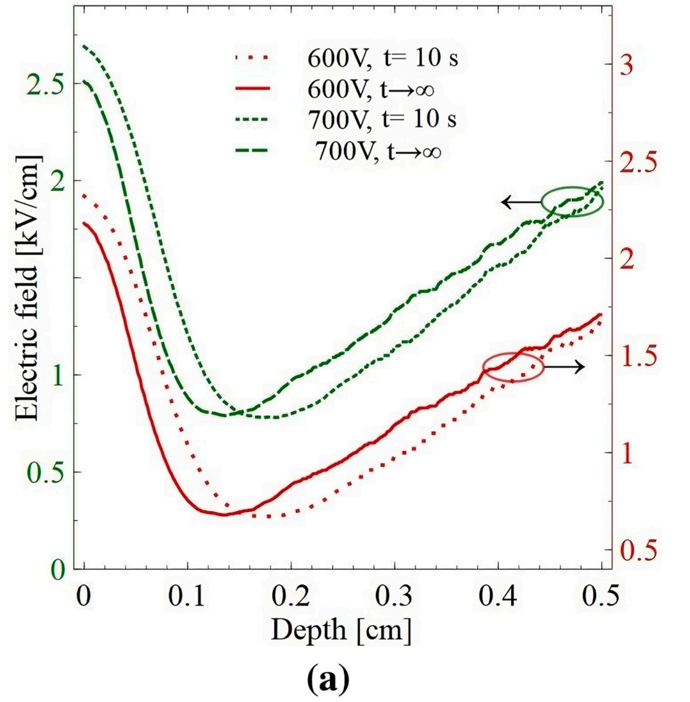

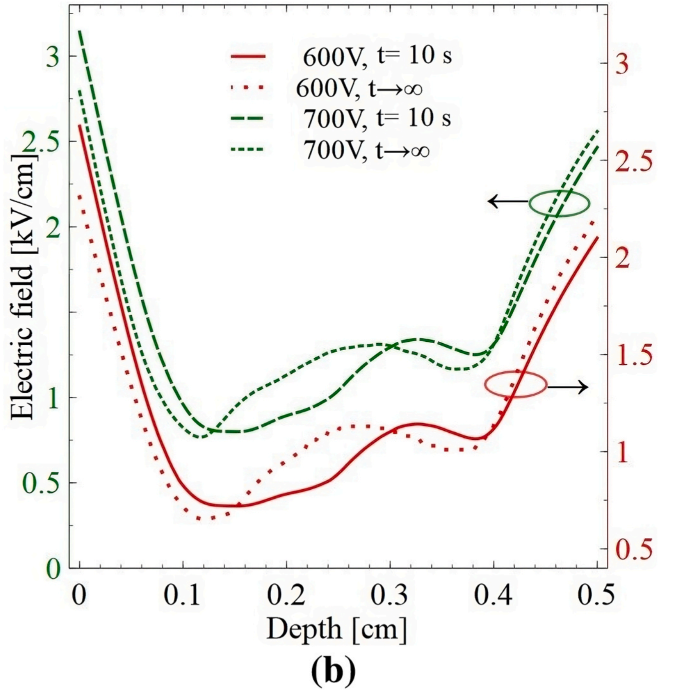

Fig. 4. Electric field profiles deduced from the TCT current pulses. For each device and bias voltage, the initial (t = 0) and steady state (t→∞) results are presented. For convenience, different voltage axes are given for the −600 V and −700 V bias conditions. (a) CZT device, (b) CMT device.

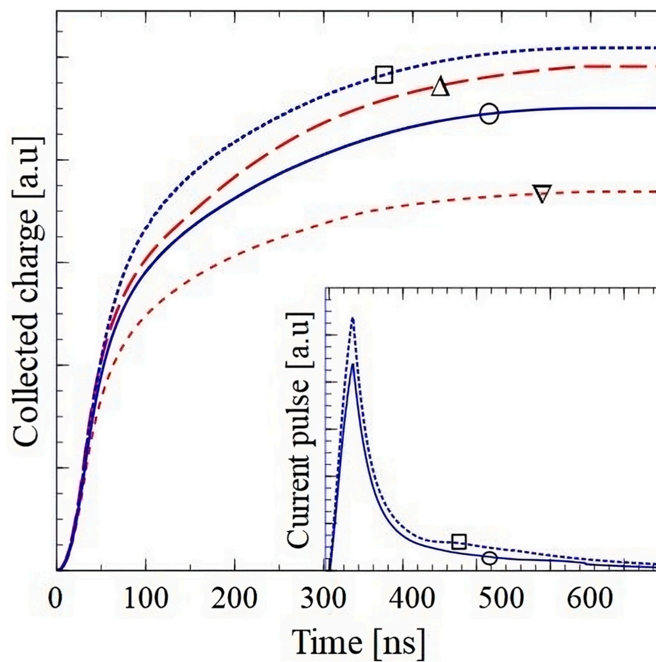

Fig. 5. Integral of the deconvoluted current TCT pulses. Circle and square denote curves for the CZT device, before and after −700 V bias-induced polarization, respectively. Signes Δ and ∇ denote curves for the CMT device, before and after −700 V bias-induced polarization, respectively. The corresponding current pulses for CZT are shown in the inset.

Declaration of competing interest

The authors declare that they have no known competing financial interests or personal relationships that could have appeared to influence the work reported in this paper.

Acknowledgments

This research was supported in part by the US-Israel Binational Science Foundation (Awards No. 2022056 and 2022779), the National Science Foundation (ECCS #2310285), PAZI (Grant 464), and NATO (MYP G6072). This work was conducted in the framework of DRD-3 collaboration at CERN.

References

[1] A.E. Bolotnikov, G.C. Camarda, G.W. Wright, R.B. James, Factors limiting the performance of CdZnTe detectors, IEEE Trans. Nucl. Sci. 52 (2005) 589–598, https://doi.org/10.1109/Tns.2005.851419.

[2] F.P. Doty, J.F. Butler, J.F. Schetzina, K.A. Bowers, Properties of cdznte crystals grown by a high-pressure bridgman method, J. Vac. Sci. Technol. B 10 (1992) 1418–1422, https://doi.org/10.1116/1.586264.

[3] S.K. Chaudhuri, M. Sajjad, J.W. Kleppinger, K.C. Mandal, Charge transport properties in CdZnTeSe semiconductor room-temperature γ-ray detectors, J. Appl. Phys. 127 (2020) 245706, https://doi.org/10.1063/5.0006227.

[4] S.K. Chaudhuri, M. Sajjad, K.C. Mandal, Pulse-shape analysis in Cd0.9Zn0.1Te0.98Se0.02 room-temperature radiation detectors, Appl. Phys. Lett. 116 (2020) 162107, https://doi.org/10.1063/5.0003646.

[5] J. Pipek, R. Grill, M. Betušiak, K. Iniewski, Modelling polarization effects in a CdZnTe sensor at low bias, Sensors 23 (2023), https://doi.org/10.3390/s23125681.

[6] A. Brovko, P. Rusian, L. Chernyak, A. Ruzin, High quality planar Cd1-xMnxTe room-temperature radiation detectors, Appl. Phys. Lett. 119 (2021), https://doi.org/10.1063/5.0060706.

[7] A. Ruzin, Simulation of compensated and overcompensated Cd1-xZnxTe, Nucl. Instrum. Methods Phys. Res. Sect. A Accel. Spectrom. Detect. Assoc. Equip. 718 (2013) 361–362, https://doi.org/10.1016/j.nima.2012.10.101.

[8] A. Brovko, A. Ruzin, Study of material uniformity in high-resistivity Cd1−xZnxTe and Cd1−xMnxTe crystals, Nucl. Instrum. Methods Phys. Res. A (2020) 958, https://doi.org/10.1016/j.nima.2019.03.051.

[9] GE HealthCare, Hamada 12A, Rabin Park Rehovot, 7670315, Israel, (n.d.). www.gehealthcare.co.il..

[10] R. Klanner, G. Kramberger, I. Mandić, M. Mikuž, M. Milovanović, J. Schwandt, Determination of the electric field in highly-irradiated silicon sensors using edge-TCT measurements, Nucl. Instrum. Methods Phys. Res. 951 (2020), https://doi.org/10.1016/j.nima.2019.162987.